Evaluation of the Detectability of Bearing Faults at Different Load Levels through the Analysis of Stator Currents

E. Martínez-Montes, L. Jiménez-Chillarón, J. Gilabert-Marzal, J. Antonino-Daviu and A. Quijano-López

Abstract— **Bearing faults are among the most relevant electrical machines failures. Their early and reliable detection can imply significant economic savings for the industry.**

This paper discusses the effects of bearing faults in the stator current, performing steady state analysis, under different load levels. A motor-generator test bench has been built in order to simulate real working conditions.

Motor current signature analysis (MCSA) is used to study steady-state regime. It is a well-known and widespread technique for detecting rotor-related faults but not so commonly used in bearing diagnosis. The objective is to study the evolution of the harmonic components in different cases of use, taking into account several types of progressive faults.

Tests were carried out with healthy and damaged induction motors under different fault severities and confirm the potential of the technique for detecting such faults. Moreover, the results show the variation of the harmonics amplitudes with the load; the paper specifies the most suitable load levels for the application of the technique.

Keywords—bearing faults, current, induction motor, MCSA, vibration.

I. INTRODUCTION

Bearing faults are among the most common failures in electric motors. Some surveys have shown that in motors rated below 4 kV, the occurrence rate of these faults is around 50% of the total failures [1-3]. Despite vibration analysis has been used with profusion for the detection of this and other mechanical failures [4-5], in some applications, the installation of vibration sensors is not easy (e.g. submersible motors), while in other cases the analysis of vibration signals may not be enough conclusive. In these cases, several authors have proposed alternative techniques for the detection of bearing faults that may overcome the problems of the vibrational analysis. In this regard, infrared thermography [6-7], stray flux analysis [8] and current analysis [9-11], among other techniques, have been suggested.

The analysis of motor currents brings interesting advantages versus other alternatives. The possibility of remote monitoring of the motor condition (the current can be measured in the motor control centre, at the secondary of current transformers of measurement devices), the simplicity of the required equipment, the low cost of the technique and the relatively broad fault coverage [12] makes it an interesting option for the detection of different faults, such as rotor problems or eccentricities. The technique has been also applied to detect several types of faults in bearings, but not so often as it has been used for detecting other failures [11]. The developed works have shown that the components introduced in the current spectrum due to bearing faults are related to those appearing in the vibration spectrum. They have also demonstrated that sometimes is difficult to detect such current harmonics due to their small amplitudes in the Fourier spectrum of the current [11]. In spite of these facts further research is needed to confirm the potential of the technique and to ratify its suitability as a complementary technology to confirm or discard the diagnosis provided by other quantities.

This work studies the detectability of different bearing failures through the evaluation of the amplitudes of different harmonic components appearing in the FFT spectrum of the steady-state current and compares the results with those obtained from the vibration spectrum. The paper also analyses the influence of the load level on the harmonic amplitudes. These results are the previous step prior to expand the analyses to transient regime.

II. EXPERIMENTAL SETUP

Several tests were performed on 5.5 kW, 400V, 4P, 50 Hz induction motor. It was tested first under healthy condition and then after causing a fault in the bearing cage and balls. The bearing employed was a radial deep groove bearing, model 6208. Its main characteristics are included in Table I. Two different operation conditions were considered: motor at no-load and motor at 90% rated load. Fig. 1 shows a scheme of the test bench.

It should be mentioned here thanks to Instituto Valenciano de Competitividad Empresarial (IVACE), as well as Fondo Europeo de Desarrollo Regional (FEDER), due to the project co-financing.

E. Martínez-Montes is with the Instituto Tecnológico de la Energía, Universitat Politècnica de València, 46022, Valencia, Spain (e-mail: ernesto.martinez@ite.es).

L. Jiménez-Chillarón is with the Instituto Tecnológico de la Energía, Universitat Politècnica de València, 46022, Valencia, Spain (e-mail: lorena.jimenez@ite.es).

J. Gilabert-Marzal is with the Instituto Tecnológico de la Energía, Universitat Politècnica de València, 46022, Valencia, Spain (e-mail: juan.gilabert@ite.es).

J. Antonino-Daviu is with the Instituto Tecnológico de la Energía, Universitat Politècnica de València, Camino de Vera s/n, 46022, Valencia, SPAIN (e-mail: joanda@die.upv.es).

A. Quijano-López is with the Instituto Tecnológico de la Energía, Universitat Politècnica de València, Camino de Vera s/n, 46022, Valencia, SPAIN (e-mail: alfredo.quijano@ite.es).

978-1-5386-2477-7/18/$31.00 ©2018 IEEE

TABLE I. 6208 BEARING DATA

Number of Balls	9
Bore Diameter	40 mm
Outer Diameter	80 mm
Pitch Circle Diameter (P_d)	60 mm
Ball Diameter (B_d)	11.906 mm
Contact angle (β)	0° (Radial)

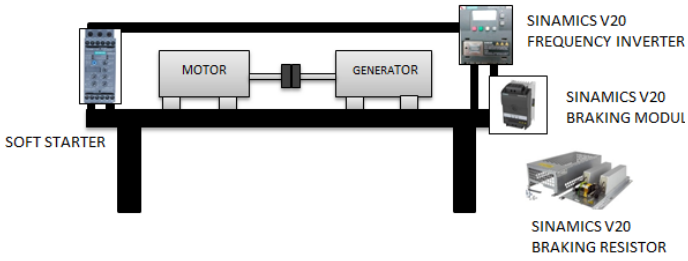

Fig. 1. Bench diagram

The test bench is based on two identical motors (one working as a motor and the other as a generator), a soft starter and a variable frequency drive (VFD). In order to simulate load and brake the motor, a braking resistor and its corresponding module are installed. The energy generated is dissipated as heat in the resistor.

The instrument employed to register the stator current was an oscilloscope and a 500 A current clamp. A sampling rate of 5 kHz was used because the expected fault frequencies were below 300 Hz.

One of the MCSA drawbacks is the dependence of fault frequencies with rotor speed. An optical speed sensor was used to measure rotor speed.

The experiments were performed on a healthy motor and, later, on the same motor with two different severities of bearing cage fault. The first fault consisted in a hole drilled in three different cage positions (Fig. 2), while in the second test all the cages were damaged. The two severities of fault will be called Damage 1 (3 holes) and Damage 2 (9 holes), respectively.

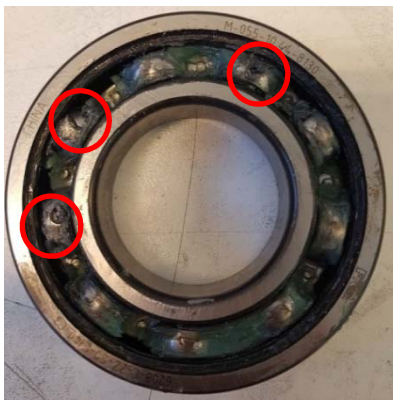

Fig. 2. Detail of damage 1 (three cage/ball positions drilled)

The first measurement procedure consists in recording the stator current at steady-state with no load. It is important to ensure constant speed and voltage supply in order to not distort the measure. For the second one, stator current is measured while the motor was operating at 90% rated load. The motor is decelerated with the help of the coupled generator, which is supplied through the variable frequency drive; the energy generated is transformed in heat in the brake resistor.

The motor was tested in each faulty condition under both loading cases. Moreover, in order to check the detectability and performance of stator current analysis, vibration measurements were also acquired during the tests with a suitable sensor.

III. FAULT FREQUENCIES

It was considered that the developed faulty cases implied the damage of both the bearing balls and the cage. The frequencies amplified by these bearing failures in the vibration spectrum are well-known and are given by expressions (1) and (2), where D_b and D_p are the diameter of the balls and the pitch diameter, respectively, f_r is the mechanical rotor frequency and β is the ball contact angle, as shown in the figure.

$$f_{ball} = \frac{D_p}{D_b} \cdot f_r \left[1 - \left(\frac{D_b}{D_p}\cos\beta\right)^2\right] \quad (1)$$

$$f_{cage} = \frac{f_r}{2} \cdot \left(1 - \frac{D_b}{D_p}\cos\beta\right) \quad (2)$$

According to [13], the relationship between these frequencies and the current spectrum is:

$$f_{bng} = |f_s \pm m f_v| \quad (3)$$

Where $m = 1, 2, 3 \ldots$, f_v is a characteristic vibration frequency, and f_s is the frequency of fundamental current harmonic.

Once fault frequencies are calculated, Fast Fourier Transform is applied to measured currents to obtain the spectrum and to track the evolution of the harmonics.

IV. RESULTS AND DISCUSSION

A. Steady-state at no load condition

Table II shows the values of the specified fault harmonic amplitudes for all faulty cases at no load condition. The results of the tests show an increment in all related fault harmonics magnitude except for $|f_s + f_{ball}|$, that didn't show a noticeable rise.

- $|f_s + f_{ball}|$: Damage 1 did not produce any significant rise. In fact, the relative variation in this state was negative. In Damage 2, is noticed a small variation increase. At first sight, this harmonic is not suitable to detect this kind of fault or the fault caused in balls was not enough.
- $|f_s - f_{ball}|$: for Damage 1, this harmonic component presented the same behaviour as the previous one. The relative variation respect of healthy state is low and negative. Respecting to Damage 2, it presented an 8.14% of variation respecting health state and 5.64% more increment than Damage 1.
- $|f_s + f_{cage}|$: relating this cage fault harmonic, a great increment is observed in Damage 1 with a relative

variation of 11.05%. in Damage 2 the magnitude grew too but it was not a progressive rise.

- $|f_s - f_{cage}|$: this second fault cage harmonic showed a more logical progression. In Damage 1 is produced a little increment in the amplitude (3.38%) and in Damage 2 this variation is highly noticeable with a percentage of 14.47%.

We must note that harmonics related to cage fault suffered a greater increment than ball fault related.

TABLE II. BEARING CURRENT HARMONICS (NO LOAD)

Formula	Frequency (Hz)	Amplitude (dB)		
		Healthy	Damage 1	Damage 2
$\|f_s + f_{ball}\|$	171.03	-80	-80.88	-78
$\|f_s - f_{ball}\|$	71.026	-67.66	-68.76	-62.15
$\|f_s + f_{cage}\|$	60.02	-81.43	-72.43	-69.34
$\|f_s - f_{cage}\|$	39.98	-76.07	-73.5	-65.06

TABLE III. BEARING CURRENT HARMONICS (NO LOAD) RELATIVE VARIATION

Formula	Frequency (Hz)	Δ (%)	
		Damage 1 / Healthy	Damage 2 / Healthy
$\|f_s + f_{ball}\|$	171.03	-1.10%	2.50%
$\|f_s - f_{ball}\|$	71.026	-1.63%	8.14%
$\|f_s + f_{cage}\|$	60.02	11.05%	14.85%
$\|f_s - f_{cage}\|$	39.98	3.38%	14.47%

B. *Steady-state at 90% rated load condition*

Table IV shows the values of the specified fault harmonic amplitudes for all faulty cases at 90% rated load condition. Similarly, as the previous case of study, all the fault concerned harmonics grew in magnitude except on $|f_s + f_{ball}|$.

- $|f_s + f_{ball}|$: as no load case, it presented a negative relative variation in Damage 1. Respecting to Damage 2, it is noticed a small increment (1.65%) but lower than no load case.
- $|f_s - f_{ball}|$: like no load regime, Damage 1 produce a slight variation (1.20%) but in this case it can be noted a great rise of for Damage 2 in comparison.
- $|f_s + f_{cage}|$: in this case, as no load regime, the relative variation respecting health state presented the principal increment in Damage 1. In Damage 2, it can be noticed a second increment but lower than Damage 1.
- $|f_s - f_{cage}|$: the behaviour of the progression of this fault component is like no load regime but in both damages the relative variation regarding health state is lower than no load case.

In comparison with no load regime, the magnitude of the harmonics is smaller, but the peaks are more visible because the spectrum with load presented a lower noise level.

In 90% load case, the variation of the amplitude is lower too but more clearly if it is compared with not representative harmonics or noise level.

TABLE IV. BEARING CURRENT HARMONICS (90% LOAD)

Formula	Frequency (Hz)	Amplitude (dB)		
		Healthy	Damage 1	Damage 2
$\|f_s + f_{ball}\|$	168.51	-80.43	-82.97	-81.76
$\|f_s - f_{ball}\|$	68.51	-84.08	-83.07	-73.1
$\|f_s + f_{cage}\|$	59.81	-78.46	-74.58	-73.85
$\|f_s - f_{cage}\|$	40.19	-81.17	-74.51	-71.16

TABLE V. BEARING CURRENT HARMONICS (90% LOAD) RELATIVE VARIATION

Formula	Frequency (Hz)	Δ (%)	
		Damage 1 / Healthy	Damage 2 / Healthy
$\|f_s + f_{ball}\|$	168.51	-3.16%	1.65%
$\|f_s - f_{ball}\|$	68.51	1.20%	13.06%
$\|f_s + f_{cage}\|$	59.81	4.95%	5.88%
$\|f_s - f_{cage}\|$	40.19	8.21%	12.33%

C. *Vibration comparison*

In order to check the detectability and the performance of the current analysis for the detection of bearing faults, the results where compared with those obtained after the analysis of vibrational data. Tables VI and VIII show the values of the amplitudes of the fault harmonics related to cage and bearing faults (equations 1 and 2) for the different faulty cases and for the both considered load levels and Tables VII and IX show the relative variation regarding health state.

- f_{ball}: in vibration analysis, the harmonic component of ball fault presented a progressive increment as the severity of the damage and this rise is more noticeable in load regime.
- f_{cage}: like ball fault component, the evolution of the amplitude is progressive with damages, but the variation is greater than ball fault.

TABLE VI. BEARING VIBRATION HARMONICS (NO LOAD)

Formula	Frequency (Hz)	Amplitude (dB)		
		Healthy	Damage 1	Damage 2
f_{ball}	121.03	-81.19	-73.54	-55.59
f_{cage}	10.02	-57.42	-48.27	-40.97

TABLE VII. BEARING VIBRATION HARMONICS (NO LOAD) RELATIVE VARIATION

Formula	Frequency (Hz)	Δ (%)	
		Damage 1 / Healthy	Damage 2 / Healthy
f_{ball}	121.03	9.42%	31.53%
f_{cage}	10.02	15.94%	28.65%

TABLE VIII. BEARING VIBRATION HARMONICS (90% RATED LOAD)

Formula	Frequency (Hz)	Amplitude (dB)		
		Healthy	Damage 1	Damage 2
f_{ball}	118.51	-73.4	-64.27	-43.98
f_{cage}	9.81	-39.34	-26.99	-19.27

TABLE IX. BEARING VIBRATION HARMONICS (90% LOAD) RELATIVE VARIATION

Formula	Frequency (Hz)	Δ (%)	
		Damage 1 / Healthy	Damage 2 / Healthy
f_{ball}	118.51	12.44%	40.08%
f_{cage}	9.81	31.39%	51.02%

In Fig. 5, it is clear the magnitude growth for the fault cage harmonic. Moreover, thanks to its higher amplitude, it is easier to track the severity of the fault. The related current harmonics have significantly lower amplitude so it is more difficult to assess the severity of the fault. The load regime presented greater amplitude values than no load regime.

Regarding ball fault harmonic, it presented lower amplitude than cage fault harmonic, and it was not as easily to identify because of the surrounding noise level.

From these analyses it can be inferred that most of the damage was done to bearing cage and the balls suffered only minor defects.

The $|f_s - f_{cage}|$ current harmonic related to cage faults was the most suitable to identify this damage due its greater amplitude variation. On the other hand, $|f_s + f_{ball}|$ component concluded to be not convenient to identify ball defects. As seen in vibrations, it seems that ball defect severity of fault was not enough to clearly detect it in current analysis.

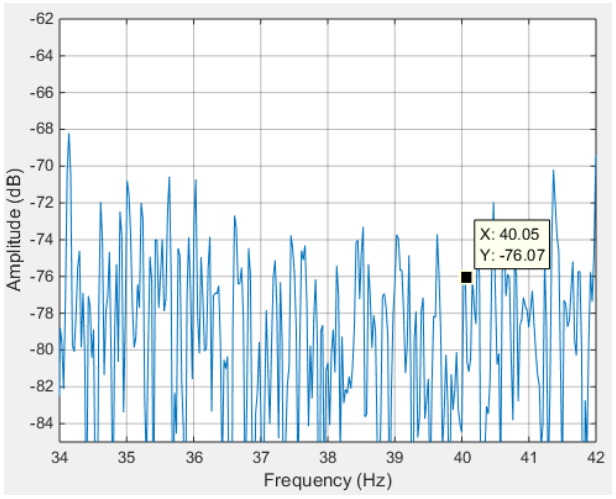

(a)

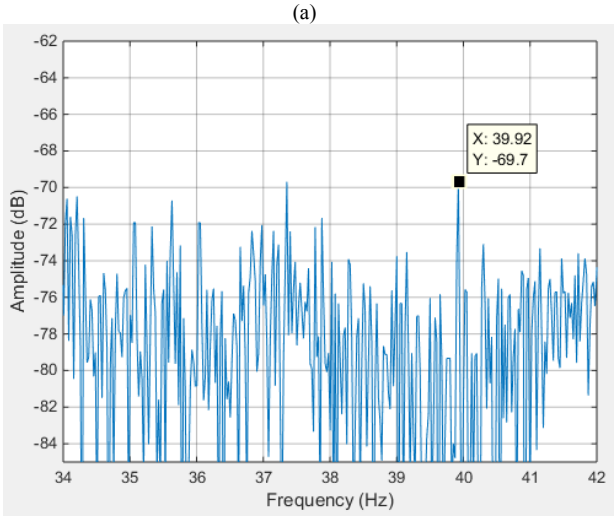

(b)

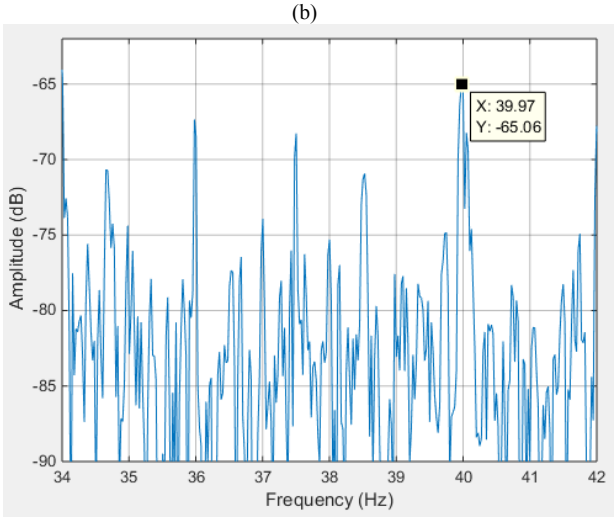

(c)

Fig. 3. Current spectrum analysis of permanent regime (no load) for (a) healthy motor, (b) damage 1, (c) damage 2

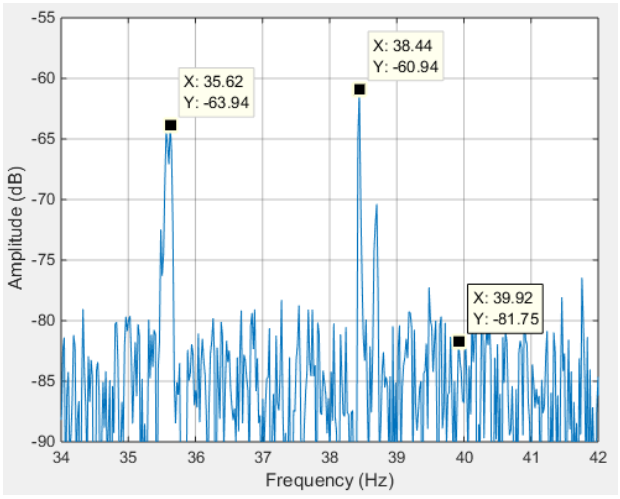

(a)

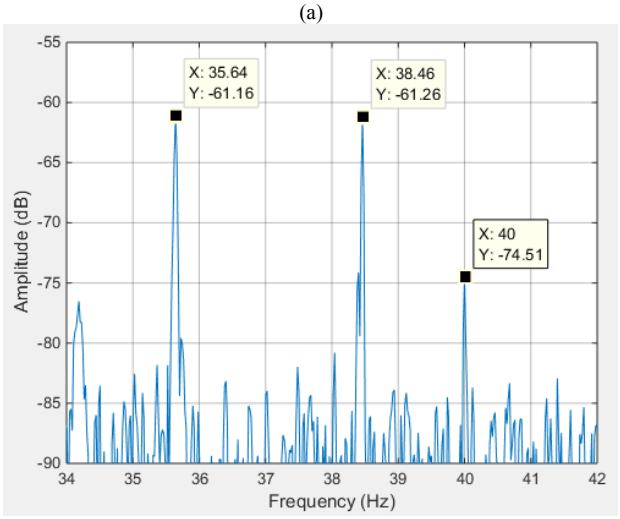

(b)

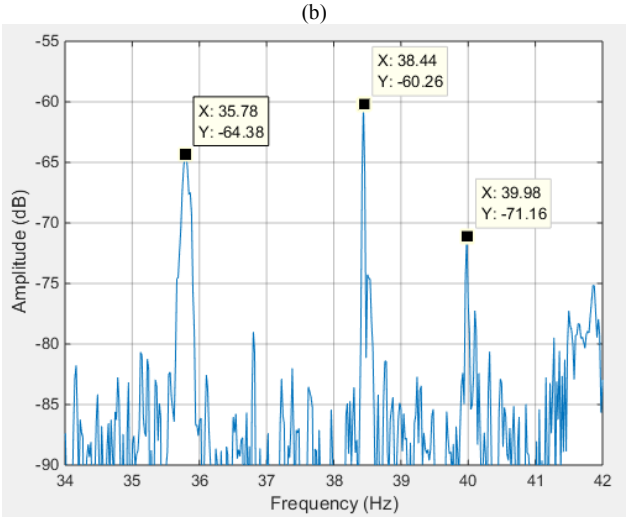

(c)

Fig. 4. Spectrum analysis of permanent regime (90% rated load) for (a) healthy motor, (b) damage 1, (c) damage 2

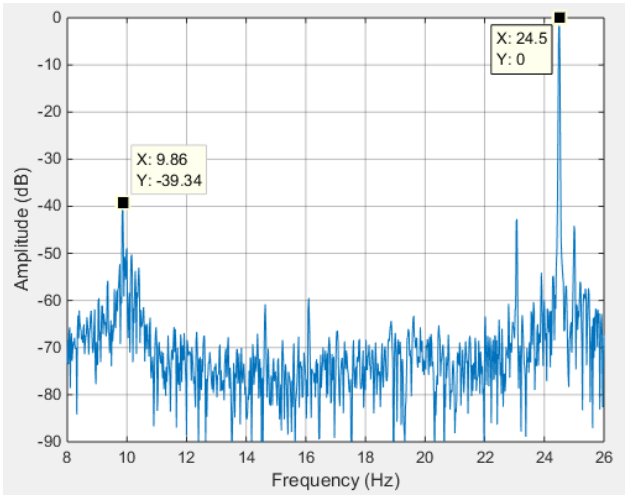

(a)

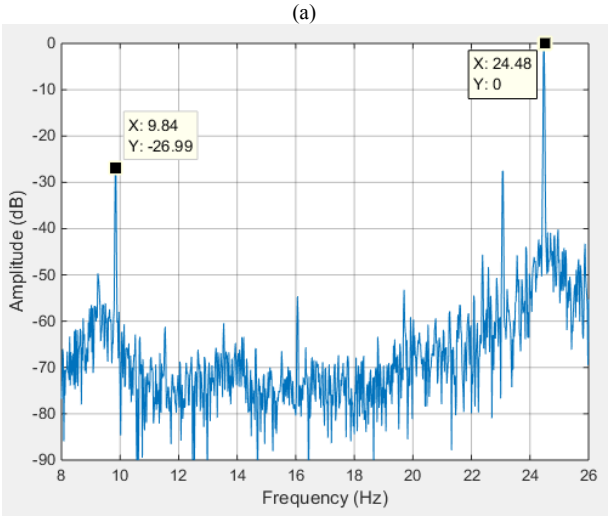

(b)

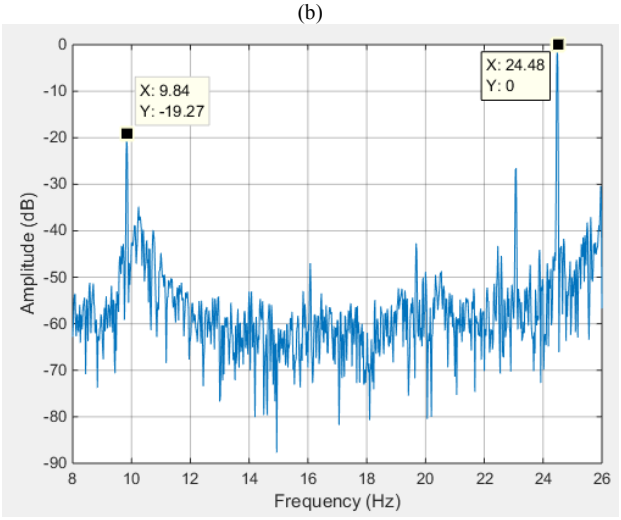

(c)

Fig. 5. Vibration spectrum analysis of permanent regime (90% rated load) for (a) healthy motor, (b) damage 1, (c) damage 2

V. CONCLUSIONS

The conclusions obtained in this paper confirm that the well-known MCSA technique can be used to detect cage and ball bearing faults. In general, the expected fault frequencies calculated grew as the severity of the fault does.

It has to be noticed that when the motor is at no load condition is more difficult to detect this increase. The absolute amplitudes are greater but the noise level is greater too so in specific cases it may be not suitable.

As the results showed, the most damaged part of the bearing was the cage while the balls were slightly damaged. The fault frequencies corresponding to cage fault suffered a more noticeable rise than the frequencies related to ball defects.

Comparison with vibration spectrum analysis showed logical results, and the fault frequencies tracked presented greater amplitude than current ones.

The current study was limited to steady state regime but time-domain analysis was performed over the transient start too. The applied technique was Short Time Fourier Transform (STFT). Though the overall harmonic level increased in magnitude, detection of specific bearing fault harmonics was difficult because their low amplitude. In this way, more research is necessary to choose the most suitable transformation and to tune and adjust it.

The results of these experiments support the idea of employing MCSA technique to detect bearing faults but with some limitations mentioned before. In any case, it is a perfectly suitable technique to complement other techniques such as vibration or thermography.

VI. REFERENCES

[1] O.V. Thorsen and M. Dalva, "Failure Identification and Analysis for High-Voltage Induction Motors in the Petrochemical Industry," *IEEE Transactions on Industry Applications*, vol. 35, no. 4, pp. 810-818, July/Aug. 1999.

[2] W.T. Thomson, M. Fenger, "Current signature analysis to detect induction motor faults" *IEEE Industry Applications Magazine*, July/August 2001, pp. 26-34.

[3] G.K. Singh y Sa'ad Ahmed Saleh Al Kazzaz, "Induction machine drive condition monitoring and diagnostic research - a survey," *Electric Power* Systems *Research,* vol. 64, no. 2, pp. 145-158, 2003.

[4] W. R. Finley, M. M. Hodowanec, W. G. Holter, "Diagnosing Motor Vibration Problems", Pulp and Paper Industry Technical Conference, 2000. Conference Record of 2000 Annual, 2000, pp. 165 – 180.

[5] N. I. Azeez and A. C. Alex, "Detection of rolling element bearing defects by vibration signature analysis: A review," in *2014 Annual International Conference on Emerging Research Areas: Magnetics, Machines and Drives (AICERA/iCMMD)*, Kottayam, 2014.

[6] E. Resendiz-Ochoa, R. A. Osornio-Rios, J. P. Benitez-Rangel, L. A. M. Hernandez and R. d. J. Romero-Troncoso, "Segmentation in thermography images for bearing defect analysis in induction motors," in *2017 IEEE 11th International Symposium on Diagnostics for Electrical Machines, Power Electronics and Drives (SDEMPED)*, Tinos, 2017.

[7] D. López-Pérez and J. Antonino-Daviu, "Application of Infrared Thermography to Failure Detection in Industrial Induction Motors: Case Stories," in *IEEE Transactions on Industry Applications*, vol. 53, no. 3, pp. 1901-1908, May-June 2017.

[8] L. Frosini, C. Harlişca and L. Szabó, "Induction Machine Bearing Fault Detection by Means of Statistical Processing of the Stray Flux Measurement," in *IEEE Transactions on Industrial Electronics*, vol. 62, no. 3, pp. 1846-1854, March 2015.

[9] J. Jung *et al*., "Monitoring Journal-Bearing Faults: Making Use of Motor Current Signature Analysis for Induction Motors," in *IEEE Industry Applications Magazine*, vol. 23, no. 4, pp. 12-21, July-Aug. 2017.

[10] W. T. Thomson and M. Fenger, "Case histories of current signature analysis to detect faults in induction motor drives," in *Electric Machines and Drives Conference, 2003. IEMDC'03. IEEE International*, 2003.

[11] H. Henao *et al*., "Trends in Fault Diagnosis for Electrical Machines: A Review of Diagnostic Techniques," in *IEEE Industrial Electronics Magazine*, vol. 8, no. 2, pp. 31-42, June 2014.

[12] S.B. Lee, E. Wiedenbrug., K. Younsi, "ECCE 2013 Tutorial: Testing and Diagnostics of Induction Machines in an Industrial Environment", presented at ECCE 2013, Denver, CO, USA, Sep 2013.

[13] R. R. Schoen, T. G. Habetler, F. Kamran and R. G. Bartfield, "Motor bearing damage detection using stator current monitoring," *IEEE Transactions on Industry Applications,* vol. 31, no. 6, pp. 1274-1279, 1995.

VII. BIOGRAPHIES

Ernesto Martínez-Montes graduated in Industrial Engineering Technologies from the Polytechnic University of Valencia in 2015. He studied a Master's degree in Industrial Engineer specialized in electric technology. In 2010, he was awarded a scholarship by the University Francisco de Vitoria and Banco Santander. He has taken several courses; one of the most relevant was a Basic Course in Nuclear Science and Technology in 2014. In 2015, he had an internship with Iberdrola Distribución Eléctrica, learning about Smart Grid and Electric Distribution in low ad medium voltage. Since 2017, he is part of the Electrical Infrastructure department of ITE as R&D Engineer, giving support to electricity sector projects.

Lorena Jiménez-Chillarón is an Industrial Engineer specialized in electric technology by the Polytechnic University of Valencia. Since 2013, she has been working at the ITE, related to energy and electricity: characterization, analysis and proposals for improving energy, development of industrial energy automation solutions, energy education and dissemination. He has also participated in projects for REE as 'Temperature monitoring in underground cables', 'Technological prospective study: Storage technologies for the operation of isolated systems with high renewable penetration'. She is currently responsible for the High Voltage and Materials area.

Juan Gilabert Marzal is an Industrial Engineer specialized in electric technology by the Polytechnic University of Valencia. He is part of the Electrical Infrastructure department as R&D Engineer. He focuses his work on National and European projects aimed at the integration of distributed resources in the electrical network and maintenance of microgrids. He has wide experience in power supply quality with electrical disturbances in electrical networks.

Jose A. Antonino-Daviu (S'04, M'08, SM'12) received his M.S. and Ph. D. degrees in Electrical Engineering, both from the Universitat Politècnica de València, in 2000 and 2006, respectively. He also received his Bs. in Business Administration from Universitat de Valencia in 2012. He was working for IBM during 2 years, being involved in several international projects. Currently, he is Associate Professor in the Department of Electrical Engineering of the mentioned University, where he develops his docent and research work. He has been invited professor in Helsinki University of Technology (Finland) in 2005 and 2007, Michigan State University (USA) in 2010, Korea University (Korea) in 2014 and Université Claude Bernard Lyon 1 (France) in 2015. He is IEEE Senior Member since 2012 and he has published over 160 contributions, including international journals, conferences and books. He is also Associate Editor of IEEE transactions on Industrial Informatics and has been Guest Editor in IEEE transactions on Industrial Electronics. He was General Co-Chair of IEEE SDEMPED 2013.

Alfredo Quijano-Lopez was born in 1960 in Valencia, Spain. He received the Electrical Engineer degree and the Ph.D. degree from Universitat Politècnica de València, in 1986 and 1992, respectively. He is the Head of the Instituto Tecnológico de la Energía. He is also a teacher and researcher at the Universitat Politècnica de València in the Electrical Engineering Department. His current research activity is focused on applied research for the Energy area and the electrical technology including renewable energies, high voltage, metrology, new materials and applications and research results transfer to companies.